Earth and Planetary Science Letters 374 (2013) 1–10

Contents lists available at SciVerse ScienceDirect

Earth and Planetary Science Letters

journal homepage: www.elsevier.com/locate/epsl

Wind as the primary driver of erosion in the Qaidam Basin, China

Alexander Rohrmann [a,*], Richard Heermance [b], Paul Kapp [c], Fulong Cai [d]

[a] Institut für Erd- und Umweltwissenschaften, University of Potsdam, 14476 Potsdam, Germany
[b] Department of Geological Sciences, California State University Northridge, Northridge, CA 91330-8266, USA
[c] Department of Geosciences, University of Arizona, Tucson, AZ 85721, USA
[d] Institute of Tibetan Plateau Research, Chinese Academy of Sciences, Beijing 100029, China

ARTICLE INFO

Article history:
Received 10 September 2012
Received in revised form
30 January 2013
Accepted 8 March 2013
Editor: G. Henderson
Available online 7 June 2013

Keywords:
wind
cosmogenic nuclide-dating
earth surface processes
Chinese Loess Plateau
climate
Asia

ABSTRACT

Deserts are a major source of loess and may undergo substantial wind-erosion as evidenced by yardang fields, deflation pans, and wind-scoured bedrock landscapes. However, there are few quantitative estimates of bedrock removal by wind abrasion and deflation. Here, we report wind-erosion rates in the western Qaidam Basin in central China based on measurements of cosmogenic ^{10}Be in exhumed Miocene sedimentary bedrock. Sedimentary bedrock erosion rates range from 0.05 to 0.4 mm/yr, although the majority of measurements cluster at 0.125 ± 0.05 mm/yr. These results, combined with previous work, indicate that strong winds, hyper-aridity, exposure of friable Neogene strata, and ongoing rock deformation and uplift in the western Qaidam Basin have created an environment where wind, instead of water, is the dominant agent of erosion and sediment transport. Its geographic location (upwind) combined with volumetric estimates suggest that the Qaidam Basin is a major source (up to 50%) of dust to the Chinese Loess Plateau to the east. The cosmogenically derived wind erosion rates are within the range of erosion rates determined from glacial and fluvial dominated landscapes worldwide, exemplifying the effectiveness of wind to erode and transport significant quantities of bedrock.

1. Introduction

Knowledge of bedrock erosion rates on Earth's surface over timescales of 10^2–10^6 yr is limited, yet fundamental in assessing the dynamics of landscape evolution and sediment production as a function of tectonic processes, climate, and lithology and their superposed forcing factors (Molnar, 2004; Whipple, 2004). Significant advances have been made in recent decades in quantifying bedrock and drainage-basin erosion rates in regions where fluvial and glacial processes dominate. Short-term landscape sedimentary flux and erosion rates (10^0–10^2 yr) have been recorded by sedimentary traps and gauging stations on rivers (Meade, 1988; Kirchner et al., 2001; Lavé and Burbank, 2004), whereas on longer timescales (10^3–10^6 yr) concentrations of in situ cosmogenic radionuclides (i.e. ^{10}Be) in fluvial sediments have been used (e.g., Granger et al., 1996; Gosse and Phillips, 2001; Von Blanckenburg, 2005, Owen et al., 2001; Portenga and Bierman, 2011). In contrast, few studies have quantified eolian erosion processes in deserts (e.g., McCauley et al., 1977; Ward and Greeley, 1984; Bristow et al., 2009; Fig. 1), particularly on timescales >5000 yr (Inbar and Risso, 2001; de Silva et al., 2010; Ruszkiczay-Rüdiger et al., 2011). This is despite the recognition of wind as an important transport agent (Pye, 1995; Uno et al., 2009), that loess is one of the most important fertilizers for plankton growth in the open ocean (Pye, 1995; Hanebuth and Henrich, 2009), and the ubiquity of wind-deflated and abraded landforms in many desert regions on Earth (Goudie, 2007) and extraterrestrial bodies such as Mars and Jupiter's moon Titan (e.g. Bridges et al., 2004; Sullivan et al., 2005; Thomson et al., 2008; Rubin and Hesp, 2009).

The in-situ produced cosmogenic nuclide ^{10}Be can be used to quantify in-situ bedrock erosion because of its long half-life ($\sim 1.3 \times 10^6$ yr), short attenuation length (<2 m), and known production rate in quartz at the Earth's surface (Lal, 1991), making it useful for studying bedrock erosion processes and assessing rates of landscape evolution in general (e.g., Bierman and Caffee, 2002; Bookhagen and Strecker, 2012). In this study, we quantify eolian erosion rates by measuring cosmogenic ^{10}Be in quartz from wind-scoured and deflated sedimentary bedrock surfaces in the Qaidam Basin (Fig. 2). We then compare our results with worldwide bedrock erosion studies in an effort to document the significance of wind as a global erosion agent.

1.1. Deflation vs. abrasion and evidence for wind erosion

In general, wind erosion is effective in arid, windy regions characterized by sparse to no vegetation cover. Wind erosion is viewed as being the result of both deflation and abrasion processes

* Corresponding author. Tel.: +49 331 977 5853; fax: +49 331 977 5700.
E-mail address: rohrmann@geo.uni-potsdam.de (A. Rohrmann).

0012-821X/$ - see front matter © 2013 Elsevier B.V. All rights reserved.
http://dx.doi.org/10.1016/j.epsl.2013.03.011

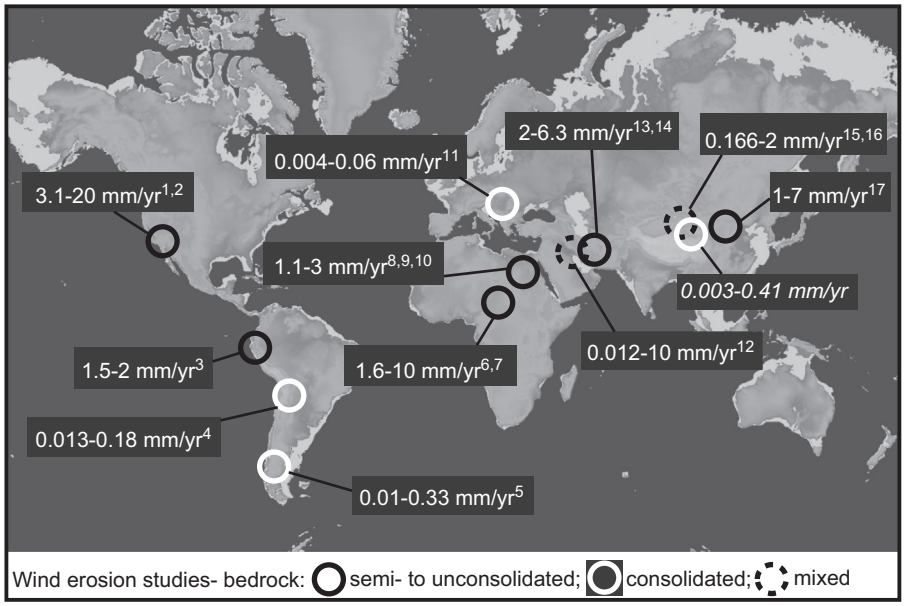

Fig. 1. Global compilation of wind erosion estimates reporting erosion by deflation (semi- to unconsolidated) and abrasion (consolidated) or both. Erosion rate estimates are based on ^{14}C-dating, optical luminescence-dating (OSL), cosmogenic ^{10}Be-dating or U–Pb dating of eroded rocks. Where no rates were reported, a conservative erosion rate was estimated using the age of the deposit and wind removed material by geometric considerations, e.g. yardang troughs; inverted channels; elevated lake beds or paleosoils above the general basin floor. Note the order of magnitude difference between wind erosion by deflation and abrasion, suggesting bedrock strength controlling the effectiveness of wind erosion. References: 1. Clarke et al. (1996), 2. Ward and Greeley (1984), 3. Beresford-Jones et al. (2009), 4. de Silva et al. (2010), 5. Inbar and Risso (2001), 6. Washington et al. (2006), 7. Bristow et al. (2009), 8. Haynes (1980), 9. Goudie et al. (1999), 10. Brookes (2003), 11. Ruszkiczay-Rüdiger et al. (2011), 12. Al-Dousari et al. (2009), 13. Krinsley (1970), 14. Kehl (2009); 15. McCauley et al. (1977), 16. Dong et al. (2012), 17. Ritley and Odontuya (2004). (For interpretation of the references to color in this figure, the reader is referred to the web version of this article.)

(Laity, 2011). Disagreements exist about the correct use of these terms, since both processes can spatially and temporally overlap and contribute to the overall wind-erosion signal. Deflation is defined here as the passive entrainment of loose material at the Earth's surface into the air-flow. In contrast, abrasion is the physical process of actively eroding material by the impact of wind-blown grains onto a bedrock surface (Goudie, 2009; Laity and Bridges, 2009). Deflation dominates wind erosion in areas where unconsolidated sediments or poorly lithified rocks are exposed at the surface. In bedrock-dominated areas floored by either consolidated sedimentary or crystalline rocks, only abrasion is able to remove material from bedrock surfaces (Laity and Bridges, 2009; Laity, 2011). However, other factors such as water (e.g. gullying, mudflow, sheet wash), temperature (freeze–thaw), and chemical weathering (salt corrosion and expansion) also impact bedrock surfaces and are able to produce loose material covering bedrock (Aref et al., 2002). Loose sediment is prone to deflation, resulting in bedrock lowering without physical abrasion. In many places it is impossible to distinguish between deflation or abrasion because of the complex relationships among weathering, climate, and bedrock lithology. Thus, information on rates and time scales of either deflation or abrasion alone are scarce.

The primary evidence for wind erosion, and specifically abrasion, in the Qaidam Basin and elsewhere are yardangs (Fig. 3A, B and E), ventifacts (Fig. 3B, foreground), and scoured, low-relief bedrock landscapes devoid of a fluvial network (Fig. 3C and D). Yardangs are wind eroded narrow ridges up to 100 m high and up to hundreds of meters in length (Hedin, 1903; Goudie, 2007). They are sculpted into poor-to-well consolidated bedrock by saltating particles that are transported by strong, uni-directional winds (McCauley et al., 1977; Dong et al., 2012). The few estimates available for the time scales of yardang formation range from thousands of years for small yardangs (1–10 m) (Halimov and Fezer, 1989) to millions of years for large yardangs ($>$ 50 m) (Goudie, 2007).

Ventifacts provide evidence for the strong abrasive power of wind at much smaller scales (Laity, 1994; Knight, 2008). Ventifacts are rocks that exhibit grooves, facets, or polishing as a result of abrasion by wind-entrained sand and typically consist of crystalline and well consolidated sedimentary rocks; they are found in most deserts and periglacial environments (Spate et al., 1995; Knight, 2002; Laity and Bridges, 2009). Reported abrasion rates associated with ventifacts are generally between 0.015 and 6.8 mm/yr (Knight 2008), although one study reported a maximum abrasion rate of 36 mm/yr over a time period of 15 yr (Sharp, 1980).

Most wind erosion occurs in the large, windy, semi-arid to arid region stretching from North Africa to central China and parts of North and South America (Fig. 1). Here, bedrock removal by wind is ubiquitous and reported wind deflation rates from semi- to unconsolidated sediment range from 1 to 20 mm/yr over short ($<$ 5000 yr) time periods (Fig. 1; Krinsley, 1970; McCauley et al., 1977; Haynes, 1980; Ward and Greeley, 1984; Clarke et al., 1996; Goudie et al., 1999; Inbar and Risso, 2001; Brookes, 2003; Ritley and Odontuya, 2004; Washington et al., 2006; Beresford-Jones et al., 2009; Bristow et al., 2009; Al-Dousari et al., 2009; Kehl, 2009; de Silva et al., 2010; Ruszkiczay-Rüdiger et al., 2011; Dong et al., 2012). Most of the presented compilation in Fig. 1 is based on studies of wind eroded features (yardangs, tree roots, channels, lake beds, lava flows) with ages quantified by ^{14}C-dating, optical luminescence-dating (OSL), and ^{40}Ar–^{39}Ar dating. There are, however, very few studies from well-lithified bedrock in areas affected by wind erosion, where abrasion should be dominant (Inbar and Risso, 2001; de Silva et al., 2010; Ruszkiczay-Rüdiger et al., 2011). Recently, Ruszkiczay-Rüdiger et al. (2011) reported cosmogenically derived eolian erosion rates between 0.003 and 0.056 mm/yr from consolidated sedimentary bedrock in the Pannonian Basin of Hungary (Fig. 1). Although this technique is promising, there have been few studies of long-term ($>$ 5000 yr) erosion rates from Central Asia (e.g. Lal et al., 2003). Here, the hyper-arid and windy conditions prevalent in northern Tibet may have enhanced eolian erosion and transport, as testified by the widespread and locally thick (hundreds of meters) accumulations of loess in eastern Asia,

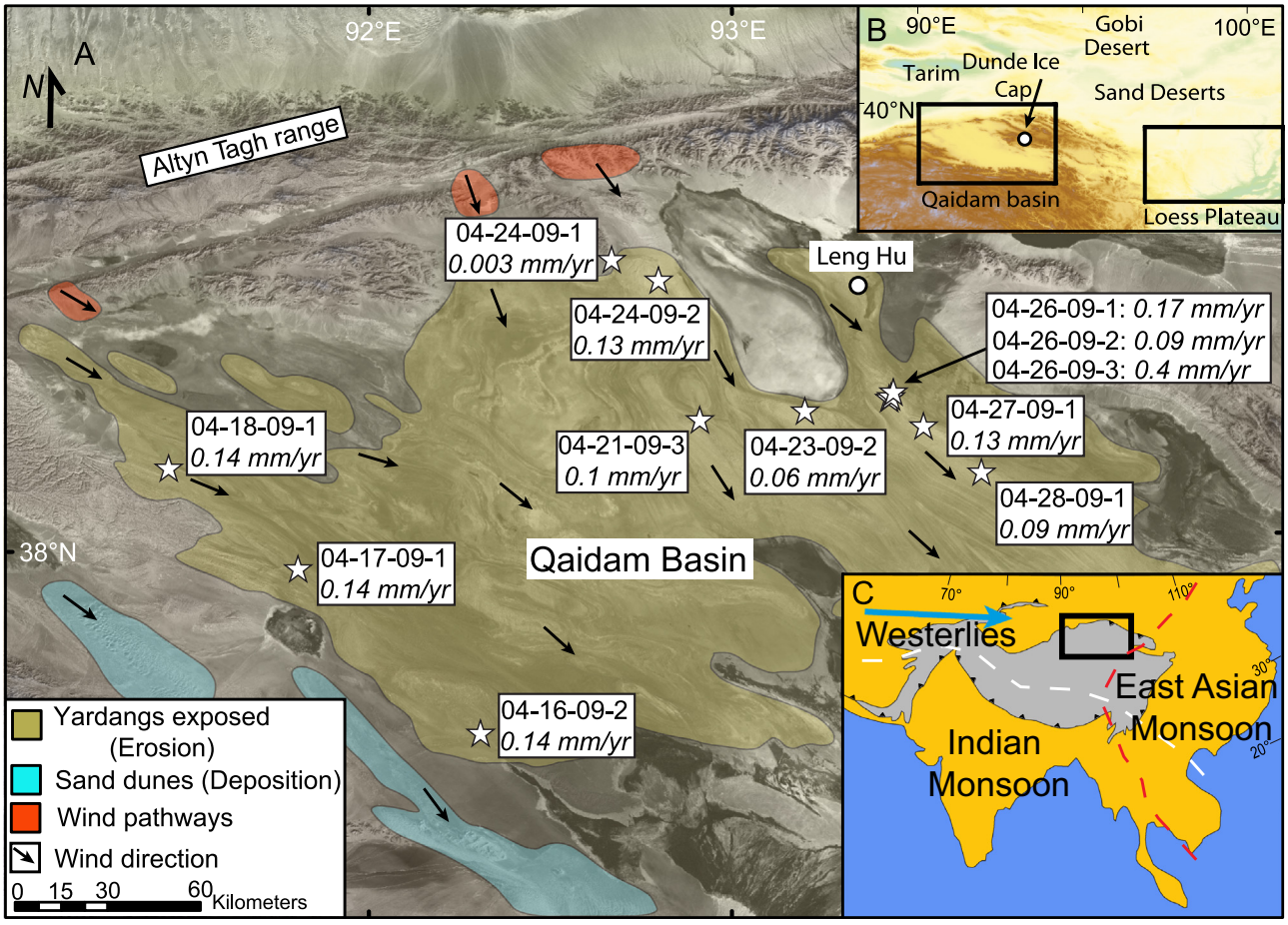

Fig. 2. (A) Landsat image of the Qaidam Basin showing the distribution of yardangs and dune fields, wind directions, and sample locations for ^{10}Be-dating. (B) Location of the Qaidam Basin and the Loess Plateau. (C) Regional overview of the major circulation systems: The Westerlies and dashed lines indicate the maximum modern extent of the Indian and East Asian Monsoon systems (after Gao, 1962).

including the Chinese Loess Plateau (CLP) (Fig. 2B) and beginning as early as 22 Myr ago (Porter, 2001; Guo et al., 2002).

1.2. Study area

The Qaidam Basin (QB) is situated at the northern edge of the Tibetan plateau and covers an area of approximately 120,000 km^2 (Fig. 2). Today, the western QB receives less than 70 mm/yr of precipitation and is one of the highest (mean elevation of ~2700 m) and driest deserts on Earth, being shielded by efficient orographic barriers (Sobel et al., 2003). In response to the ongoing Indo-Asian collision, the basin is being shortened in a NE–SW direction (Tapponnier et al., 2001) and its floor exposes folded, friable sedimentary rock of the Miocene Shang Youshashan, Shizigou and Qigequan formations (e.g. Kapp et al., 2011, Wang et al., 2012). The Miocene Formations (Shang Youshashan and Shizigou) are characterized by sandstone and conglomerate lenses (i.e. deltaic facies) that pinch out laterally into deeper-water siltstone and shale (i.e. lacustrine facies; Heermance et al., 2013). Based on its low internal relief (<300 m), internal drainage, intermontane basin setting, and thick accumulations of Cenozoic basin fill, it generally has been inferred that the QB has been dominated by sediment accumulation rather than erosion until recently (Zhou et al., 2006), even though roughly one-third of the modern basin floor ($\sim 3.88 \times 10^4$ km^2) exposes yardangs carved in folded sedimentary strata (Fig. 2; Kapp et al., 2011). The predominant wind direction in the basin is from the northwest to southeast, while in the eastern part of the basin the predominant wind direction is more easterly, parallel to the orientation of the >5000-m-high basin-bounding mountain ranges to the north and south (Fig. 2). The wind eroded and quartz-rich strata throughout the basin make it ideal to quantify wind erosion and bedrock removal rates with cosmogenic ^{10}Be. In this study, we define wind erosion as being the sum of deflationary and abrasive processes acting on a surface, resulting in lowering and removal of bedrock in a hyperarid landscape marginally affected by rainfall events and fluvial processes. These conditions are met by the QB, where hundreds to thousands of vertical meters of consolidated basin fill may have been removed by wind over the last 2.8 million years (Kapp et al., 2011).

2. Methods

2.1. Cosmogenic nuclide dating

Terrestrial cosmogenic nuclides are isotopes that form from the interaction of cosmic particles with elements in Earth's atmosphere and surface. In particular, the cosmogenic nuclide ^{10}Be forms from the interaction of cosmogenic particles with quartz (Lal, 1991). Production of ^{10}Be decays exponentially with depth as the penetration of cosmic rays attenuates to zero a few meters below the ground surface. Furthermore, ^{10}Be is radiogenic with a half-life of $\sim 1.3 \times 10^6$ yr (Nishiizumi et al., 2007) and thus is not present in buried rocks more than a few million years old. The concentration of ^{10}Be in rocks at the Earth's surface is

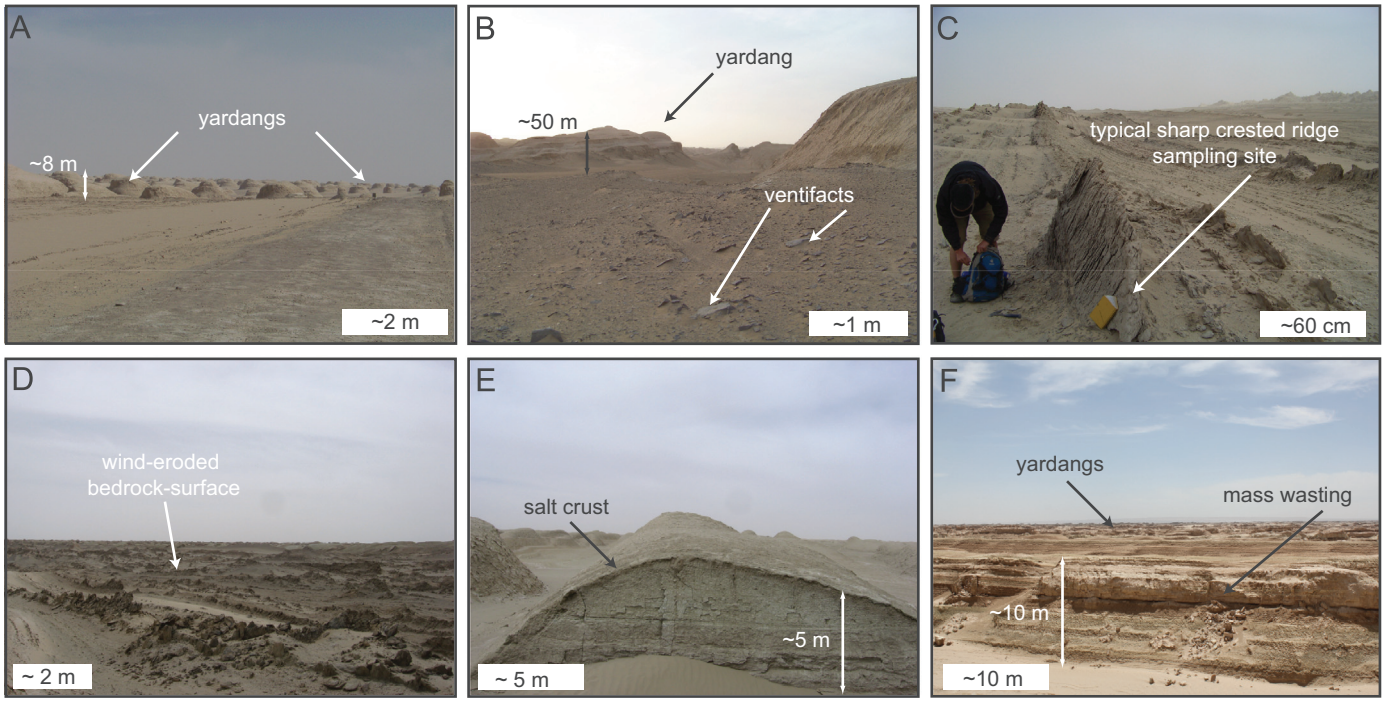

Fig. 3. Photos from the study area showing: (A) Yardang field with 5–8 m high yardangs. (B) Foreground: desert pavement/ventifacts, with 10–30 cm clasts. Background: ~25–50 m high yardangs and inter-yardang trough. (C) Typical sharp-crested ridge sampling side with no visible fluvial network. (D) Vast wind scoured-bedrock landscape exposing sampled Miocene bedrock. (E) Road-cut through a yardang, exposing a ~20-cm-thick layer of salt crust, armoring the landscape from wind erosion. (F) Picture was taken after a strong but very rare rain-event. The yardangs are ~10 m high. Mass-wasting is seen on the side of the front yardang in form of debris-flows and rock fall.

therefore a function of the production rate, the radioactive decay, and the local erosion rate. Erosion rate can be determined because the production rate (itself a function of altitude and latitude) and the decay rate of the target isotope is known (Lal, 1991). This technique has been applied to bedrock within many landscapes (e.g., Bierman and Turner, 1995; Brown et al., 1995, Nishiizumi et al., 1991; Small et al., 1997), including on bedrock exposed across the Tibetan Plateau (Lal et al., 2003). The calculated erosion rates are essentially a measure of the time required to remove ~2 m of bedrock, which corresponds to the absorption depth for most cosmic rays in typical rocks. Our calculations are based on the assumption of steady-state erosion, although as discussed later (Section 4.1) it is likely that erosion rates have varied significantly over time.

The 250–500 μm sand fraction of quartz was separated from twelve samples distributed across the western QB and processed following the methodology of Kohl and Nishiizumi (1992). Samples were spiked with an in-house, low ^{10}Be-concentration carrier (^{10}Be/^{9}Be 4×10^{-15} made from Ural Mts. phenacite) at the University of Arizona. ^{10}Be/^{9}Be ratios were measured at the Acceleration Mass Spectrometer at Lawrence Livermore National Laboratories, Berkeley, CA. Erosion rates were calculated using the CRONUS calculator (Balco and Rovey, 2008) and account for ^{10}Be production at the latitude and elevation of the sample location and any potential shielding of the sample site from cosmic radiation by nearby topography.

2.2. Sampling method and sites

Twelve bedrock samples were collected for ^{10}Be analysis from the western QB (Fig. 2). Here, the basin floor exposes actively growing anticlines, where strata form wind scoured bedrock surfaces or are sculpted into yardangs (Fig. 3A–F). Eleven samples were collected from medium- to coarse-grained sandstones within Miocene fluvio-lacustrine strata. The age of the strata for all our samples is greater than 5.3 Ma based on regional mapping and stratigraphic correlation with magnetostratigraphy (Heermance et al., 2013; Wang et al., 2012). Miocene bedrock was targeted because these rocks would have been buried to sufficient depths (more than hundreds of meters) for at least the last 5 Myr, such that the ^{10}Be inheritance produced during prior exposure should have decayed to near zero concentration. Most of the targeted samples were located along sharp crested ridges. The ridges in turn are elevated above the mean basin floor, show evidence of wind scouring, and lack any fluvial network (see supplementary data for photos of individual sample sites). By sampling sharp crested ridges that stand above the landscape, we avoided the effects of surface-water runoff that would be focused into low spots within the landscape. Moreover, sharp crested ridges represent points in the landscape that have been lowered to a lesser degree, and thus lower rate, than their surroundings, and therefore should yield erosion rate minima assuming an initially flat landscape. It is possible that infrequent rain events (Fig. 3F) impact the local erosion signal, although the lack of any continuous catchment area implies that erosion due to runoff, particularly on the tops of the ridges, was very low. Moreover, rain events are not capable of removing sediment from the basin because of the basin's internal drainage; any eroded material must ultimately have been removed from the basin by wind. The basin floor is almost scoured clean of sediment, implying the removal of locally produced sediment by deflation was more efficient than the amount of loose sediment generated by wind abrasion and other erosional/weathering processes.

Three of the twelve samples were taken from inclined hillslope surfaces. These samples have a higher probability to having been affected by hill-slope and mass-wasting processes in contrast to the remaining samples, and we take these into account during our interpretation of the erosion rates. Sample 4-28-09-1 was taken from a 60° dipping side-slope of a yardang. Samples 4-17-09-1 and 4-26-09-1 were collected from well consolidated bedrock exposed on steep ($>70°$) cliff faces. In order to assess variations in wind erodibility as a function of bedrock cohesiveness/strength, we also

analyzed one granite sample (4-24-09-1) exposed along the northwestern margin of the QB adjacent to the Altyn Tagh Range (Fig. 2).

3. Results

^{10}Be concentrations for the twelve samples ranged between 6.291×10^4 and 1.054×10^7 atoms/g of quartz (Table 1). These concentrations, when corrected for topographic shielding, provide cosmogenically derived bedrock erosion rates of 0.003–0.4 mm/yr (Fig. 4 and Table 1). Under the assumption of steady-state erosion, the rates would integrate erosion over a time period of up to 15,000 yr for the Miocene bedrock samples and 500,000 yr for the Altyn-Tagh granite—the time required to remove the upper 2 m of material (zone of ^{10}Be accumulation). Nine of the twelve samples have bedrock removal rates that cluster between 0.09 and 0.17 mm/yr within average of 0.125 mm/yr (Fig. 4). Among these nine samples, three (4-17-09-1, 4-26-09-1 and 4-28-09-1) were collected from 50–70° dipping surfaces, and thus the results are more ambiguous to interpret due to their prominent position with respect to mass-wasting activity. Furthermore, applying shielding correction to these samples is difficult because the surface may have catastrophically failed over the time span of ^{10}Be accumulation. The effect of mass wasting processes for these three samples (samples 4-17-09-1, 4-26-09-1 and 4-28-09-1) is not detectible on the basis of anomalously high erosion rates compared to samples collected from ridges on regionally flat landscapes, however, and implies that hillslope processes may be negligible compared to wind erosion in most places within the western QB. Overall, sampling on sharp crested ridges within overall flat landscapes is advised for future studies to rule out potential mass wasting events during the exposure of the sampled surface.

Whereas most of our samples clustered tightly around 0.125 mm/yr, samples 4-23-09-2 (hard sandstone) and 4-24-09-1 (granite sample) yielded lower rates (0.057 and 0.003 mm/yr, respectively) and 4-26-09-3 yielded a higher rate (0.4 mm/yr; Fig. 4). These discrepancies can be accounted for by variations in rock strength. Sample 4-23-09-2 is a very coarse grained, well-consolidated sandstone and provides a lower bedrock erosion rate of 0.057 mm/yr, lower than the average (0.09–0.17 mm/yr). This reflects greater resistance to bedrock erosion, which is further supported by its prominent high-elevation position relative to most of the basin floor. The Altyn-Tagh granite 4-24-09-1 exhibits the greatest rock strength of all samples and correspondingly shows the strongest resistance to erosion with an erosion rate of 0.003 mm/yr. This very low erosion rate is consistent with other ^{10}Be-erosion rates determined for granitic bedrock exposed elsewhere adjacent to the Qaidam Basin and on the Tibetan Plateau (Lal et al., 2003, Fig. 4). The highest erosion rate of 0.4 mm/yr was obtained from sample 4-26-09-3, collected from a yardang located on a limb of an actively growing anticline in the northwestern part of the basin near Leng Hu (Fig. 2).

4. Discussion

4.1. Temporal variability of Qaidam wind erosion rates

The erosion rates presented here, with the average being ~0.125 mm/yr, are based on the assumption of steady-state erosion over the past ~15,000 yr, resulting in ~2 m of bedrock removal. Based on a number of paleoclimatic and geologic arguments, however, it is likely that erosion in the QB was higher than our determined erosion rates in other parts of the wind-eroded basin and during the last glacial episode.

First, all samples were exclusively collected from indurated and erosion-resistant Miocene bedrock exposed along the axes of anticlines, in contrast to the less consolidated and younger strata exposed along syncline axes. Wind erosion rates would be expected to be greater in troughs that have been lowered to a greater extent than the intra-basin ridges. We did not sample and analyze the more friable Plio-Quaternary strata exposed in the syncline axes because rocks younger than Miocene presumably contain inherited ^{10}Be acquired prior to and during deposition, and would further underestimate overall basin-wide erosion rates.

Second, considering the regional paleoclimatic evidence (e.g. Thompson et al., 1989; Liu et al., 1994; Shao et al., 2005; Herzschuh, 2006; Zhao et al., 2007, 2010; Wang et al., 2008), the greatest factor influencing wind erosion rates and their temporal variability is climate change controlling changes in wind patterns and vegetation cover. Wind patterns and moisture supply in the QB are strongly influenced by the westerlies and in part by the East-Asian summer and winter monsoon system (Fig. 2C; Bryson, 1986). Changes in these systems have resulted in complex impacts on the erosional system. The available climatic records indicate drier conditions during the last glacial in northern Tibet compared to a much wetter Holocene (Herzschuh, 2006). This pattern is attributed to a weakening and southward shift of the monsoonal systems during glacial periods, which suppressed moisture supply to NE-Tibet, and a Holocene northward migration of the monsoon with progressively wetter conditions during warming (Thompson et al., 2005; Wang et al., 2008). The southward shift of the monsoonal system in glacial times may have been associated with

Table 1
Cosmogenic nuclide results.

Sample ♯	Rock Type	Location	Latitude (N)	Longitude (E)	Altitude (m)	^{10}Be concentration (atoms/g)	^{10}Be concentration error (atoms/g)	Erosion rate [a] (mm/yr)	Erosion rate uncertainty [a] (mm/yr)
4-16-09-2	Sandstone	Crested ridge	37.516	92.296	3050	228,195	7771	0.138	0.012
4-17-09-1	Sandstone	70°-Cliff	37.967	92.796	2972	107,720	4022	0.144	0.011
4-18-09-1	Sandstone	Crested ridge	38.243	92.441	2778	191,675	6902	0.145	0.012
4-21-09-3	Sandstone	Crested ridge	38.375	92.897	2786	292,823	9714	0.093	0.008
4-23-09-2	Sandstone	Crested ridge	38.400	92.185	2792	485,639	15,921	0.057	0.005
4-24-09-1	Granite	Crested ridge	38.815	92.655	3306	10,544,507	331,768	0.003	0.001
4-24-09-2	Sandstone	Crested ridge	38.758	92.784	2975	234,360	8438	0.133	0.012
4-26-09-1	Sandstone	70°-Cliff	38.434	92.416	2878	86,380	3272	0.171	0.014
4-26-09-2	Sandstone	Crested ridge	38.436	92.422	2997	358,772	15,145	0.087	0.008
4-26-09-3	Sandstone	Yardang top	38.445	92.419	2851	62,905	2700	0.401	0.035
4-27-09-1	Sandstone	Crested ridge	38.358	92.510	2988	242,840	8721	0.128	0.011
4-28-09-1	Sandstone	60° slope-mount	38.232	92.669	2838	214,256	7704	0.092	0.008

[a] The erosion rate is calculated based on steady-state erosion (see text).

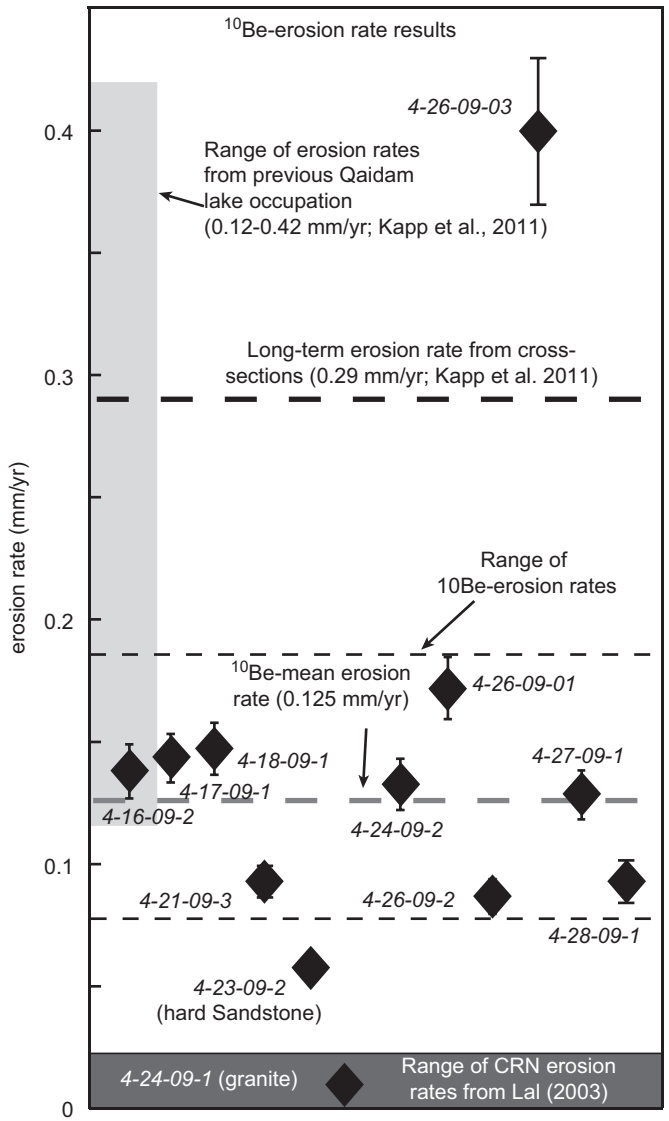

Fig. 4. ^{10}Be-erosion rate results with 2-σ-error bars, showing range of results and mean-erosion rate. In addition, Qaidam erosion rate estimates from yardangs carved into initially flat laying lake sediments (light gray box) and cross-sections both from Kapp et al. (2011). Dark gray box shows, for comparison, the erosion rate range for granite samples from the Qaidam Basin and the Tibetan Plateau (Lal et al., 2003).

a $>10^{\circ}$ southward shift of the polar jet stream compared to its modern position (Shin et al., 2003; Toggweiler and Russell, 2008; Kapp et al., 2011; Pullen et al., 2011). The more southerly position of the jet stream during glacial periods would have favored the passage of large, low-pressure systems over the QB, which likely resulted in high wind speeds that, together with less vegetation cover during dry glacial periods, were able to efficiently erode large quantities of sediment. The increase in wind erosion and removal of material from the western QB during glacials is recorded in the Dunde ice cap located in the Qilian Shan $\sim$100 km east of the study area (Fig. 2b; Thompson et al., 1989). The ice core shows large quantities of dust input throughout the last glacial, followed by a dramatic reduction at the onset of the Holocene. Lake, pollen, and tree-ring records from the QB itself indicate aridity in the basin throughout the glacial until today, not capturing the Holocene northward shift and increased monsoonal precipitation (Phillips et al., 1993; Zhao et al., 2007, 2010). The prolonged aridity may be explained by the high present-day evapo-transpiration potential of 2000–3000 mm/yr, which also existed during the glacial periods (Phillips et al., 1993). The overall high evapo-transpiration must have suppressed any incoming high moisture fluxes during the Holocene. It is surprising, however, that even as the Holocene climate in the QB stayed dry and favorable to produce dust, dust fluxes and thus wind erosion were dramatically reduced as evidenced by the Dunde ice core record (Thompson et al., 1989). Simultaneously, dust emission and loess accumulation in the CLP also decreased substantially as evidenced by the start of paleosol formation at 9.3 ± 0.5 ka (Porter, 2001; Yaofeng et al., 2008). The greatest factor for the Holocene reduction in the dust flux and in turn wind erosion may have been the changing wind pattern and reduction of wind speeds in response to a northward shift in the polar jet stream.

Another factor that may have decreased Holocene wind erosion in the QB is the local formation of salt crust. Today, parts of the Qaidam, including yardangs and depressions, are covered with a 10–35 cm thick salt crust (Fig. 3E), especially where the salt-rich Qigequan Formation (Pleistocene) is exposed at the surface. Here, the salt-crust potentially armored the landscape and protected the underlying material from erosion. Formation of the salt crust in the QB may have coincide with the massive increase of chloride in the Dunde ice-core record at the Pleistocene–Holocene transition $\sim$10,000 years ago and in turn a significant reduction of dust input (Thompson et al., 1989), resulting in lower erosion rates in areas affected by salt-crust formation throughout the Holocene.

On the basis of the above mentioned climatic and geologic considerations it is reasonable that wind-erosion rates were significantly higher during the last glacial period compared to our determined ^{10}Be-erosion rates covering the past $\sim$15,000 yr. This is in line with the dust deposition history in the Dunde ice core and the CLP, both of which show major changes with the start of the Holocene around $\sim 10^4$ yr. In general, such a history would translate into higher wind erosion rates during previous glacial conditions compared to determined mean ^{10}Be bedrock erosion rate of 0.125 mm/yr. This interpretation is in line with basin-wide averaged erosion rates from the QB, based on geological cross-sections (0.29 mm/yr, Kapp et al., 2011) (Fig. 4). Likewise, 50 m high yardangs carved into 120–400 ka flat laying lake deposits, imply similarly high minimum averaged erosion rates (0.12–0.42 mm/yr, Kapp et al., 2011, Fig. 4).

In summary, variable climate conditions (a drier climate, less vegetation, and stronger wind speeds during the LGM compared to the Holocene) within the QB should directly translate to variable wind erosion rates over time. Similar variability in wind erosion also occurred in southern Argentina, where yardangs are carved into an early Pleistocene lava flow that is overlain by a 1000 yr old lava flow that does not show signs of wind erosion (Inbar and Risso, 2001) or in the Western Pannonian Basin in Hungary, where times of strong wind erosion activity (during glacial periods) varied with times of enhanced vegetation, landform stability, and subdued erosion (during interglacial periods) (Ruszkiczay-Rüdiger et al., 2011). These correlations imply a global climate impact during the last glacial maximum on wind erosion rates worldwide.

4.2. The link to the Chinese Loess Plateau

Despite Quaternary wind erosion in the Qaidam Basin and the presence of the Chinese Loess Plateau located downwind from and east of the QB (Fig. 2B, Porter, 2001), few studies have argued for a source–sink relationship between the two areas (Liu et al., 1994; Wu et al., 2010; Kapp et al., 2011). A recent study of wind-blown zircons from the CLP has identified the QB and the northern Tibetan plateau as the principal source areas (Pullen et al., 2011). Kapp et al. (2011) suggested that wind erosion in the QB has been active since 2.6 Ma and estimated from geological cross-sections

that roughly two-thirds of the loess plateau volume can be explained by the volume of eroded sedimentary basin fill. Today, roughly one-third ($\sim 3.88 \times 10^4$ km^2) of the modern basin floor exposes yardangs. If we consider our mean basin-wide averaged wind-erosion rate of 0.125 mm/yr, we estimate a wind eroded volume of $\sim 1 \times 10^4$ km^3 (erosion rate (0.125 mm/yr) $\times$ start of erosion (2.6 Ma) $\times$ modern yardang area ($\sim 3.88 \times 10^4$ km^2)). The result is equivalent to a volume of one-sixth of the CLP (Loess plateau volume $\sim 6 \times 10^4$ km^3). However, if the atmospheric circulation pattern was different than today (Shin et al., 2003; Toggweiler and Russell, 2008; Kapp et al., 2011; Pullen et al., 2011) and wind erosion rates were higher during glacial periods in line with QB basin-wide averaged erosion rates from geological cross-sections and yardangs cut in original flat lying lake sediments (Kapp et al., 2011), erosion rates may have been higher over the long-term. This would result in higher volumes of eroded basin material and would account for a higher amount of the Loess Plateau volume, whereas the remaining material could have been derived from northern Tibet and the Gobi and adjacent sand deserts during interglacial periods (Pullen et al., 2011). Overall, the cosmogenically derived volumetric estimates of eroded QB material support the hypothesis that the QB is a major source of loess for the CLP (Bowler et al., 1987; Kapp et al., 2011; Pullen et al., 2011).

4.3. Global comparison and control on wind erosion rates

The wind erosion rates determined for the western QB constitute some of the highest erosion rates measured using in-situ cosmogenic nuclide dating in an arid environment (Fig. 1 and Table 1). This contrasts with ^{10}Be bedrock erosion rates in the hyper-arid Atacama Desert of Chile which vary between 0.0003 and 0.006 mm/yr (Nishiizumi et al., 2005), cosmogenic nuclide erosion rates from the Tibetan Plateau of < 0.03 mm/yr (Lal et al., 2003), and typical erosion rates for bedrock surfaces not affected by fluvial or glacial processes (~ 0.01–0.05 mm/yr; see Small et al., 1997 for a review of other studies). The range of Qaidam bedrock erosion rates (0.05–0.4 mm/yr) agrees well with rates of calculated wind abrasion and yardang development in well-consolidated bedrock from Argentina, Chile, Hungary, Saudi-Arabia and other parts of China (0.01–0.18 mm/yr) (Fig. 1: red circles; Inbar and Risso, 2001; de Silva et al., 2010; Al-Dousari et al., 2009; Ruszkiczay-Rüdiger et al., 2011; Dong et al., 2012), but are much lower than global wind deflation rates (1–20 mm/yr) (Fig. 1: green circles; e.g. McCauley et al., 1977; Goudie et al., 1999; Brookes, 2003; Washington et al., 2006; Al-Dousari et al., 2009; Bristow et al., 2009). The stark difference in reported wind erosion rates may be attributed to the different bedrock strengths of the eroding material (unconsolidated vs. weakly consolidated and well consolidated). Overall, in comparison with other global studies on yardang development in bedrock-floored deserts, the QB is by far the most erosive, perhaps with the exception of the Lut desert of Iran, where yardangs, having relief of > 100 m, have formed in consolidated late Pleistocene strata (Krinsley, 1970; Kehl, 2009).

To further investigate the differences between abrasion and deflation and their individual control on wind-erosion efficiency, we plotted the global estimates of wind erosion rates against rock strength of wind eroded material (Fig. 5). We used the range of rock tensile strengths determined by Marin and Sauer (1954), Kulhawy (1975), and Larma and Vutukuri (1978), as a measure of bedrock strength and resistance to erosion. There exists a clear break in the efficiency of wind erosion as bedrock tensile strength

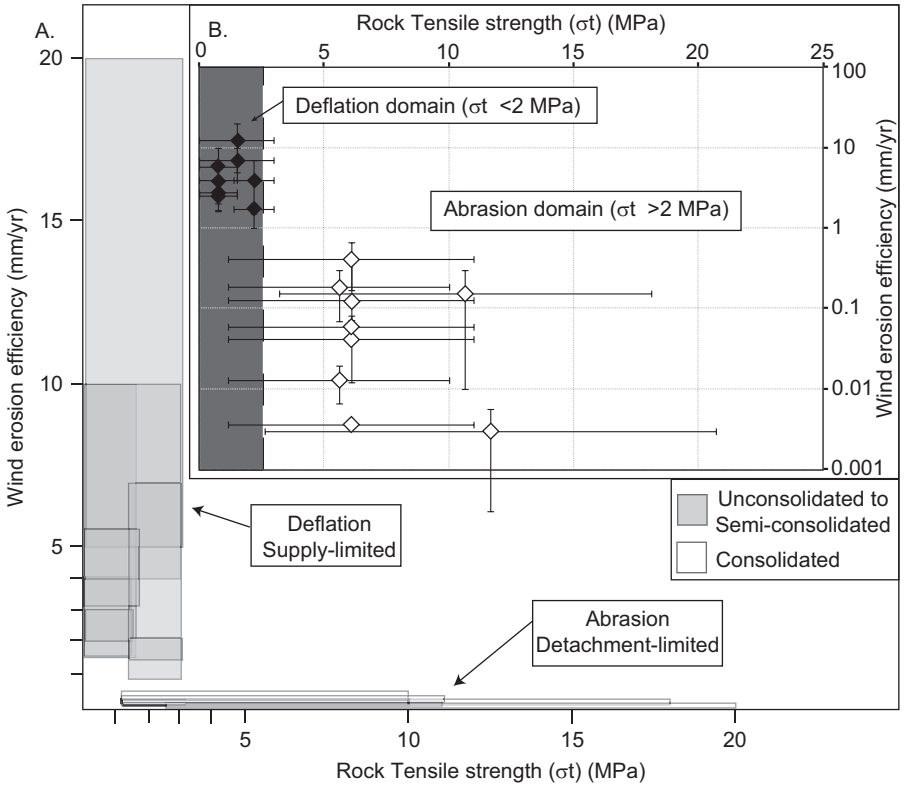

Fig. 5. (A) Plot of wind erosion rate versus rock tensile strength using the global compilation of wind erosion rates in Fig. 1 and determined bedrock strengths of the eroding material by Marin and Sauer (1954), Kulhawy (1975), and Larma and Vutukuri (1978). Each box represents a single study and its range of wind erosion estimates and error, as well as the range of determined tensile strengths for the eroding material. Note the large rate difference between semi- to unconsolidated (gray) and consolidated material (white). (B) Wind erosion rate is plotted in log-space versus rock tensile strength with error bars. Different colors (black—deflation; white—abrasion) represent individual wind erosion domains controlled by deflation or abrasion.

increases (Fig. 5A and B). Consolidated bedrock, with greater tensile strength, has much lower wind-erosion rates of ~0.003–0.667 mm/yr compared to semi- to unconsolidated material, which range between 1 and 20 mm/yr. The result is not surprising since deflation should be dominant in semi- to unconsolidated material, whereas deflation is limited in strong material where the generation of loose material available for deflation is supply limited. In contrast, consolidated rocks, having high bedrock strengths, should only erode by the mode of wind abrasion, but in turn at much lower rates. On the basis of Fig. 5b, we define domains of predominantly deflation ($\sigma_t < 2$ MPa) or abrasion ($\sigma_t > 2$ MPa) as a function of rock tensile strength (Fig. 5b). The exact rock tensile strength at which this transition occurs needs to be systematically investigated in future studies. The relationships depicted in Fig. 5b, however, provide a first-order assessment. In summary, deflation processes should be supply-limited, since high rates of up to 20 mm/yr are not sustainable over long periods. This short-term process contrasts with wind abrasion, which is detachment-limited. In general, wind deflation and abrasion should be viewed as two modes of wind-erosion that are not fully distinct from each other, but are controlled by bedrock strength.

4.4. Significance of wind erosion and global sediment flux

The role of wind as an erosive agent in significantly contributing to global sedimentary flux has not been analyzed in depth (Goudie, 2008). Nonetheless, wind erosion as shown may be very effective in eroding material in some deserts, and possibly as equally effective as fluvial erosion in many other environments. Our cosmogenically derived wind erosion rates (average 0.125 mm/yr) are within the range of those reported worldwide from glacial (~0.08–1000 mm/yr) and fluvial (~0.001–100 mm/yr) dominated regions (Koppes and Montgomery, 2009). Wind erosion rates are on the same order as glacial erosion rates obtained from the mountains of the Pacific Northwest of North America, for example (~0.1 mm/yr). Compared to fluvial erosion rates, wind erosion rates are on the same order as fluvial erosion measured in rivers from the Apennines (~0.1 mm/yr), they are higher than fluvial erosion rates in cratons (< 0.1 mm/yr), and they are comparable to the lower end of the spectrum of fluvial erosion of rivers in tectonically active regions.

The effectiveness of wind as an erosional agent is further highlighted by the thick loess deposits of the CLP as well as large accumulations of dust offshore in the Pacific, Atlantic, and Indian oceans (Porter, 2001; Rea et al., 1998; Hanebuth and Henrich, 2009). Loess production itself is today viewed as a direct product of sand grain abrasion and subsequent grain-size reduction, because during the impact of saltating grains the grain size is reduced (Anderson, 1986; Crouvi et al., 2008). Under modern conditions, only sand seas and deflating lake basins have been recognized to be major sources and production areas of loess in mid-latitude deserts where loess is not sourced from glacial environments (Crouvi et al., 2010, Enzel et al., 2010). Our study shows that areas with yardangs are also a major source for loess. It is in this type of environment that material is actively being eroded and subsequently experiencing a grain size reduction from sand to fine silt due to the impact of saltating grains during wind storm events.

5. Conclusions

New ^{10}Be cosmogenic erosion rates obtained from well consolidated Miocene sedimentary rocks on the Qaidam Basin floor yield eolian bedrock erosion rates between 0.05 and 0.4 mm/yr, with a mean rate of ~0.125 mm/yr. Rates are highest along an actively growing anticlines in Miocene sedimentary strata, and lowest in resistant, granitic bedrock, with a rate of 0.003 mm/yr. Our results provide the first quantification of eolian bedrock erosion rates associated with yardang fields in central Asia. The virtual absence of fluvial erosion on the sharp crested ridges and yardang tops sampled suggest that the erosion is dominated by wind processes. Paleoclimate and geologic evidence, together with the enhanced formation of salt crust at the start of the Holocene, suggest that wind erosion rates may have been highly variable and were likely significantly higher during past, especially during cold, glacial conditions. Our study identifies the Qaidam Basin as an environment of severe wind erosion and implies that wind erosion can occur at rates comparable to fluvial and glacial processes in specific climatic and tectonic settings. Based on existing global long-term (> 5000 yr) datasets, the Qaidam Basin is one of the most erosive deserts on Earth. Calculated volumes of eroded material from the Qaidam Basin during the Quaternary suggest that at least 16% and potentially more of the Chinese Loess Plateau deposits may have been derived from the Qaidam Basin. In addition, a relationship between wind deflation and abrasion rates was established in relation to the bedrock strength of the eroding material. Our new data will help to calibrate numerical models of wind erosion and yardang development and contribute to a better understanding of abrasion vs. deflation processes in general.

Acknowledgments

The research was funded by donors to the American Chemical Society Petroleum Research Fund (Grant ACS PRF#48729-ND8). We gratefully acknowledge the help of Andrew McCallister during sample collection. Furthermore, we thank Jay Quade for the use of the cosmogenic isotope lab at the University of Arizona, and Bodo Bookhagen for assistance with sample preparation advice. In addition, we thank the DFG-Leibniz Center for Surface Processes and Climate Studies at the Universität Potsdam, Germany, for their support.

Appendix A. Supporting information

Supplementary data associated with this article can be found in the online version at http://dx.doi.org/10.1016/j.epsl.2013.03.011.

References

Al-Dousari, A.M., Al-Elaj, M., Al-Enezi, E., Al-Shareeda, A., 2009. Origin and characteristics of yardangs in the Um Al-Rimam depressions (N Kuwait). Geomorphology 104, 93–104.
Anderson, R.S., 1986. Erosion profiles due to particles entrained by wind: application of an eolian sediment-transport model. Geol. Soc. Am. Bull. 97, 1270–1278.
Aref, M.A.M., El-Khoriby, E., Hamdan, M.A., 2002. The role of salt weathering in the origin of the Qattara Depression, Western Desert, Egypt. Geomorphology 45, 181–195.
Balco, G., Rovey, C.W., 2008. An isochron method for cosmogenic-nuclide dating of buried soils and sediments. Am. J. Sci. 308, 1083–1114.
Beresford-Jones, D., Lewis, H., Boreham, S., 2009. Linking cultural and environmental change in Peruvian prehistory: geomorphological survey of the Samaca Basin, Lower Ica Valley, Peru. Catena 78, 234–249.
Bierman, P., Turner, J., 1995. ^{10}Be and ^{26}Al evidence for exceptionally low rates of Australian bedrock erosion and the likely existence of Pre-Pleistocene landscapes. Quat. Res. 44, 378–382.
Bierman, P.R., Caffee, M., 2002. Cosmogenic exposure and erosion history of Australian bedrock landforms. Geol. Soc. Am Bull. 114, 787–803.
Bookhagen, B., Strecker, M.R., 2012. Spatiotemporal trends in erosion rates across a pronounced rainfall gradient: examples from the southern Central Andes. Earth Planet. Sci. Lett. 327–328, 97–110.

Bowler, J.M., Chen, K., Yuan, B., 1987. Systematic variations in loess source areas: evidence from Qaidam and Qinghai basins, western China. In: Tungsheng, L. (Ed.), Aspects of Loess Research. China Ocean Press, Beijing, pp. 39–51.
Bridges, N.T., Laity, J.E., Greeley, R., Phoreman, J., Eddlemon, E.E., 2004. Insights on rock abrasion and ventifact formation from laboratory and field analog studies with applications to Mars. Planet. Space Sci. 52, 199–213.
Bristow, C.S., Drake, N., Armitage, S., 2009. Deflation in the dustiest place on Earth: the Bodélé Depression, Chad. Geomorphology 105, 50–58.
Brookes, I.a., 2003. Geomorphic indicators of Holocene winds in Egypt's Western Desert. Geomorphology 56, 155–166.
Brown, E.T., Stallard, R.F., Larsen, M.C., Raisbeck, G.M., Yiou, F., 1995. Denudation rates determined from the accumulation of in situ-produced ^{10}Be in the Luquillo experimental forest, Puerto Rico. Earth Planet. Sci. Lett. 129, 193–202.
Bryson, R.A., 1986. Airstream climatology of Asia. In: Proceedings of International Symposium on the Qinghai-Xizang Plateau and Mountain Meteorology. American Meteorological Society, Boston, Ma, pp. 604–617.
Clarke, M.L., Wintle, A.G., Lancaster, N., 1996. Infra-red stimulated luminescence dating of sands from the Cronese Basins, Mojave Desert. Geomorphology 17, 199–205.
Crouvi, O., Amit, R., Enzel, Y., Porat, N., Sandler, A., 2008. Sand dunes as a major proximal dust source for late Pleistocene loess in the Negev Desert, Israel. Quat. Res. 70, 275–282.
Crouvi, O., Amit, R., Enzel, Y., Gillespie, A.R., 2010. Active sand seas and the formation of desert loess. Quat. Sci. Rev. 29, 2087–2098.
de Silva, S.L., Bailey, J.E., Mandt, K.E., Viramonte, J.M., 2010. Yardangs in terrestrial ignimbrites: synergistic remote and field observations on Earth with applications to Mars. Planet. Space Sci. 58, 459–471.
Dong, Z., Lv, P., Lu, J., Qian, G., Zhang, Z., Luo, W., 2012. Geomorphology and origin of Yardangs in the Kumtagh Desert, Northwest China. Geomorphology 139–140, 145–154.
Enzel, Y., Amit, R., Crouvi, O., Porat, N., 2010. Abrasion-derived sediments under intensified winds at the latest Pleistocene leading edge of the advancing Sinai–Negev erg. Quat. Res. 74, 121–131.
Gao, Y., 1962. Some Problems on East-Asia Monsoon. Science Press, Beijing in Chinese.
Gosse, J.C., Phillips, F.M., 2001. Terrestrial in situ cosmogenic nuclides: theory and application. Quat. Sci. Rev. 20, 1475–1560.
Goudie, A.S., Stokes, S., Cook, J., Samieh, S., El-Rashidi, O.A., 1999. Yardang landforms from Kharga Oasis, south-western Egypt. Z. Geomorphol. Suppl.-Bd 116, 97–112.
Goudie, A.S., 2007. Mega-Yardangs: a Global Analysis. Geogr. Compass 1, 65–81.
Goudie, A.S., 2008. The history and nature of wind erosion in deserts. Annu. Rev. Earth Planet. Sci. 36, 97–119.
Goudie, A.S., 2009. Dust storms: recent developments. J. Environ. Manage. 90, 89–94.
Granger, D.E., Kirchner, J.W., Finkel, R., 1996. Spatially averaged long-term erosion rates measured from in-situ-produced cosmogenic nuclides in alluvial sediment. J. Geol. 104, 249–257.
Guo, Z.T., Ruddiman, W.F., Hao, Q.Z., Wu, H.B., Qiao, Y.S., Zhu, R.X., Peng, S.Z., Wei, J.J., Yuan, B.Y., Liu, T.S., 2002. Onset of Asian desertification by 22 Myr ago inferred from loess deposits in China. Nature 416, 159–163.
Halimov, M., Fezer, F., 1989. Eight yardang types in central Asia. Z. Geomorphol. 33, 205–217.
Hanebuth, T.J.J., Henrich, R., 2009. Recurrent decadal-scale dust events over Holocene western Africa and their control on canyon turbidite activity (Mauritania). Quat. Sci. Rev. 28, 261–270.
Haynes, C.V., 1980. Geologic evidence of pluvial climates in the El Nabta area of the Western Desert, Egypt. In: Wendorf, F., Schild, R. (Eds.), Prehistory of the Eastern Sahara. Academic Press, New York, pp. 353–371.
Hedin, S., 1903. Central Asia and Tibet. Hurst and Blackeet, London, p. 1272.
Heermance, R.V., Pullen, A., Kapp, P., Garzione, C.N., Bogue, S., Ding, L., Song, P., 2013. Climatic and tectonic controls on sedimentation and erosion during the Pliocene- Quarternary in the Qaidam Basin (China). Geological Society of America Bulletin 125, 833–856, http://dx.doi.org/10.1130/B30748.1.
Herzschuh, U., 2006. Palaeo-moisture evolution in monsoonal Central Asia during the last 50,000 years. Quat. Sci. Rev. 25, 163–178.
Inbar, M., Risso, C., 2001. Holocene yardangs in volcanic terrains in the southern Andes, Argentina. Earth Surf. Processes Landforms 26, 657–666.
Kapp, P., Pelletier, J.D., Rohrmann, A., Heermance, R., Russell, J., Ding, L., 2011. Wind erosion in the Qaidam basin, central Asia: implications for tectonics, paleoclimate, and the source of the Loess Plateau. GSA Today 21, 4–10.
Kehl, M., 2009. Quaternary climate change in Iran—the state of knowledge. Erdkunde 63, 1–17.
Kirchner, J.W., Finkel, R.C., Riebe, C.S., Granger, D.E., Clayton, J.L., King, J.G., Megahan, W.F., 2001. Mountain erosion over 10 yr, 10 k.y., and 10 m.y. time scales. Geology 29, 591–594.
Knight, J., 2002. Wind abrasion (ventifaction) on Donegal and Oregon coasts and implications for the sediment dynamics of coastal systems. J. Coastal Res SI 36, 441–449.
Knight, J., 2008. The environmental significance of ventifacts: a critical review. Earth-Sci. Rev. 86, 89–105.
Kohl, C.P., Nishiizumi, K., 1992. Chemical isolation of quartz for measurement of in-situ-produced cosmogenic nuclides. Geochim. Cosmochim. Acta 56, 3583–3587.
Koppes, M.N., Montgomery, D.R., 2009. The relative efficacy of fluvial and glacial erosion over modern to orogenic timescales. Nat. Geosci. 2, 644–647.
Krinsley, D.B., 1970. A geomorphological and paleoclimatological study of the playas of Iran70–800, US Geological Survey Final Report, Contract PRO CP.
Kulhawy, F.H., 1975. Stress deformation properties of rock and rock discontinuities. Eng. Geol. 9, 327–350.
Laity, J.E., 1994. Landforms of aeolian erosion. In: Abrahams, A.D., Parsons, A.J. (Eds.), Geomorphology of Desert Environments. Chapman & Hall, London, pp. 506–535.
Laity, J.E., Bridges, N.T., 2009. Ventifacts on Earth and Mars: analytical, field, and laboratory studies supporting sand abrasion and windward feature development. Geomorphology 105, 202–217.
Laity, J.E., 2011. Wind erosion in drylands. In: Thomas, D.S (Ed.), Arid Zone Geomorphology: Process, Form and Change in Drylands. John Wiley & Sons, Oxford, UK, pp. 539–568.
Lal, D., 1991. Cosmic ray labeling of erosion surfaces: in situ nuclide production rates and erosion models. Earth Planet. Sci. Lett. 104, 424–439.
Lal, D., Harris, N.B.., Sharma, K.K., Gu, Z., Ding, L., Liu, T., Dong, W., Caffee, M.W., Jull, A.J.., 2003. Erosion history of the Tibetan Plateau since the last interglacial: constraints from the first studies of cosmogenic ^{10}Be from Tibetan bedrock. Earth Planet. Sci. Lett. 217, 33–42.
Larma, R.D., Vutukuri, V.S., 1978. Handbook on Mechanical Properties of Rocks, vol. II. Trans. Tech. Publ., Schwitzerland.
Lavé, J., Burbank, D., 2004. Denudation processes and rates in the Transverse Ranges, southern California: erosional response of a transitional landscape to external and anthropogenic forcing. J. Geophys. Res. 109, 1–31.
Liu, C.Q., Masuda, A., Okada, A., Yabuki, S., Fan, Z.-L., 1994. Isotope geochemistry of Quaternary deposits from the arid lands in northern China. Earth Planet. Sci. Lett. 127, 25–38.
Marin, J., Sauer, J.A., 1954. Strengths of Materials. Macmillan, New York.
McCauley, J.F., Breed, C.S., Grolier, M.J., 1977. Yardangs. In: Doehring, D.O. (Ed.), Geomorphology in Arid Regions. George Allen and Unwin, Boston, pp. 233–269.
Meade, R.H, 1988. Movement and storage of sediment in river systems. In: Lerman, A., Meybeck, M. (Eds.), Physical and Chemical Weathering in Geochemical Cycles. Kluwer Academic Publishers, Dordrecht, Netherlands, pp. 165–179.
Molnar, P., 2004. Late Cenozoic increase in accumulation rates of terrestrial sediment: how might climate change have affected erosion rates? Annu. Rev. Earth Planet. Sci. 32, 67–89.
Nishiizumi, K., Kohl, C.P., Arnold, J.R., Klein, J., Fink, D., Middleton, R., 1991. Cosmic ray produced ^{10}Be and ^{26}Al in Antarctic rocks: exposure and erosion history. Earth Planet. Sci. Lett. 104, 440–454.
Nishiizumi, K., Caffee, M.W., Finkel, R.C., Brimhall, G., Mote, T., 2005. Remnants of a fossil alluvial fan landscape of Miocene age in the Atacama Desert of northern Chile using cosmogenic nuclide exposure age dating. Earth Planet. Sci. Lett. 237, 499–507.
Nishiizumi, K., et al., 2007. Absolute calibration of Be-10 AMS standards. Nucl. Instrum. Methods Phys. Res. Sect. B 258 (2), 403–413.
Owen, L. a., Gualtieri, L., Finkel, R.C., Caffee, M.W., Benn, D.I., Sharma, M.C., 2001. Cosmogenic radionuclide dating of glacial landforms in the Lahul Himalaya, northern India: defining the timing of Late Quaternary glaciation. J. Quat. Sci. 16, 555–563.
Phillips, F.M., Zreda, M.G., Ku, T.-lung, Luo, S., Huang, Q.I., Elmore, D., Kubik, P.W., Sharma, P., 1993. ^{230}Th/^{234}U and ^{36}Cl dating of evaporite deposits from the western Qaidam Basin, China: implications for glacial-period dust export from Central Asia. Geol. Soc. Am. Bull. 105, 1606–1616.
Portenga, E.W., Bierman, P.R., 2011. Understanding Earth's eroding surface with ^{10}Be. GSA Today 21, 4–10.
Porter, S., 2001. Chinese loess record of monsoon climate during the last glacial–interglacial cycle. Earth-Sci. Rev. 54, 115–128.
Pullen, A., Kapp, P., McCallister, A.T., Chang, H., Gehrels, G.E., Garzione, C.N., Heermance, R.V., Ding, L., 2011. Qaidam Basin and northern Tibetan Plateau as dust sources for the Chinese Loess Plateau and paleoclimatic implications. Geology 39, 1031–1034.
Pye, K., 1995. The nature, origin and accumulation of loess. Quat. Sci. Rev. 14, 653–667.
Rea, D.K., Snoeckx, H., Joseph, L.H., 1998. Late Cenozoic eolian deposition in the North Pacific: Asian drying, Tibetan uplift, and cooling of the northern hemisphere. Paleoceanography 13, 215–224.
Ritley, K., Odontuya, E., 2004. Yardangs and Dome Dunes Northeast of Tavan Har. Gobi, Mongolia.
Rubin, D.M., Hesp, P.A., 2009. Multiple origins of linear dunes on Earth and Titan. Nat. Geosci. 2, 653–658.
Ruszkiczay-Rüdiger, Z., Braucher, R., Csillag, G., Fodor, L.I., Dunai, T.J., Bada, G., Bourlés, D., Müller, P., 2011. Dating Pleistocene aeolian landforms in Hungary, Central Europe, using in situ produced cosmogenic ^{10}Be. Quat. Geochronol. 6, 515–529.
Shao, X., Huang, L., Liu, H., Liang, E., Fang, X., 2005. Reconstruction of precipitation variation from tree rings in recent 1000 years in Delingha, Qinghai. Sci. China Ser. D: Earth Sci. 48, 939–949.
Sharp, R.P., 1980. Wind-driven sand in Coachella Valley, California: further data Wind-driven sand in Coachella Valley, California: Further data. Geol. Soc. Am. Bull. 91, 724–730.
Shin, S.I., Otto-Bliesner, B., Brady, E.C., Kutzbach, J.E., Harrison, S.P., 2003. A simulation of the Last Glacial Maximum climate using the NCAR-CCSM. Clim. Dyn. 20, 127–151.
Small, E.E., Anderson, R.S., Repka, J.L., Finkel, R., 1997. Erosion rates of alpine bedrock summit surfaces deduced from in situ ^{10}Be and ^{26}Al. Earth Planet. Sci. Lett. 150, 413–425.

Sobel, E.R., Hilley, G.E., Strecker, M.R., 2003. Formation of internally drained contractional basins by aridity-limited bedrock incision. J. Geophys. Res. 108, 1–23.
Spate, A.P., Burgess, J.S., Shevlin, J., 1995. Rates of rock surface lowering, Princess Elizabeth Land, Eastern Antarctica. Earth Surf. Processes Landforms 20, 567–573.
Sullivan, R., Banfield, D., Bell, J.F., Calvin, W., Fike, D., Golombek, M., Greeley, R., Grotzinger, J., Herkenhoff, K., Jerolmack, D., Malin, M., Ming, D., Soderblom, L.a, Squyres, S.W., Thompson, S., Watters, W.a., Weitz, C.M., Yen, A., 2005. Aeolian processes at the Mars Exploration Rover Meridiani Planum landing site. Nature 436, 58–61.
Tapponnier, P., Zhiqin, X., Roger, F., Meyer, B., Arnaud, N., Wittlinger, G., Jingsui, Y., 2001. Oblique stepwise rise and growth of the Tibet plateau. Science 294, 1671–1677.
Thompson, L.G., Mosley-Thompsonm, E., Davis, M.E., Bolzan, J.F., Dai, J., Yao, T., Gundestrup, N., Wu, X., Klein, L., Xie, Z., 1989. Holocene-Late Pleistocene climatic ice core records from Qinghai-Tibetan Plateau. Science 246, 274–477.
Thompson, L.G., Davis, M.E., Mosley-Thompson, E., Lin, P.-N., Henderson, K.A., Mashiotta, T.A., 2005. Tropical ice core records: evidence for asynchronous glaciation on Milankovitch timescales. J. Quat. Sci. 20, 723–733.
Thomson, B.J., Bridges, N.T., Greeley, R., 2008. Rock abrasion features in the Columbia Hills, Mars. J. Geophys. Res. 113, 1–13.
Toggweiler, J.R., Russell, J., 2008. Ocean circulation in a warming climate. Nature 451, 286–288.
Uno, I., Eguchi, K., Yumimoto, K., Takemura, T., Shimizu, A., Uematsu, M., Liu, Z., Wang, Z., Hara, Y., Sugimoto, N., 2009. Asian dust transported one full circuit around the globe. Nat. Geosci. 2, 557–560.
Von Blanckenburg, F., 2005. The control mechanisms of erosion and weathering at basin scale from cosmogenic nuclides in river sediment. Earth Planet. Sci. Lett. 237, 462–479.
Wang, Y., Cheng, H., Edwards, R.L., Kong, X., Shao, X., Chen, S., Wu, J., Jiang, X., Wang, X., An, Z., 2008. Millennial- and orbital-scale changes in the East Asian monsoon over the past 224,000 years. Nature 451, 1090–1093.
Wang, Y., Zhen, J., Zhang, W., Li, S., Liu, X., Yang, X., Liu, Y., 2012. Cenozoic uplift of the Tibetan Plateau: evidence from the tectonic-sedimentary evolution of the western Qaidam Basin. Geosci. Front. 3 (2), 175–187.
Ward, A.W., Greeley, R., 1984. Evolution of the yardangs at Rogers Lake, California. Geol. Soc. Am. Bull. 95, 829–837.
Washington, R., Todd, M.C., Lizcano, G., Tegen, I., Flamant, C., Koren, I., Ginoux, P., Engelstaedter, S., Bristow, C.S., Zender, C.S., Goudie, a.S., Warren, a., Prospero, J.M., 2006. Links between topography, wind, deflation, lakes and dust: the case of the Bodélé Depression, Chad. Geophys. Res. Lett. 33, 1–4.
Whipple, K.X., 2004. Bedrock rivers and the geomorphology of active orogens. Annu. Rev. Earth Planet. Sci. 32, 151–185.
Wu, G., Zhang, C., Zhang, X., Tian, L., Yao, T., 2010. Sr and Nd isotopic composition of dust in Dunde ice core, Northern China: implications for source tracing and use as an analogue of long-range transported Asian dust. Earth Planet. Sci. Lett. 299, 409–416.
Yaofeng, J., Chunchang, H., Jiangli, P., Junjie, N., 2008. Chronology of the Holocene loess-paleosol section and its deposition and pedogenesis on the south of Chinese Loess Plateau. J. Geogr. Sci. 18, 425–442.
Zhao, Y., Yu, Z., Chen, F., Ito, E., Zhao, C., 2007. Holocene vegetation and climate history at Hurleg Lake in the Qaidam Basin, northwest China. Rev. Palaeobot. Palynol. 145, 275–288.
Zhao, Y., Yu, Z., Liu, X., Zhao, C., Chen, F., Zhang, K., 2010. Late Holocene vegetation and climate oscillations in the Qaidam Basin of the northeastern Tibetan Plateau. Quat. Res. 73, 59–69.
Zhou, J., Xu, F., Wang, T., Cao, a., Yin, C., 2006. Cenozoic deformation history of the Qaidam Basin, NW China: results from cross-section restoration and implications for Qinghai–Tibet Plateau tectonics. Earth Planet. Sci. Lett. 243, 195–210.